Pressure-Induced Transformations in Diborane: A Raman Spectroscopic Study

Chitra Murli[†] and Yang Song*

Department of Chemistry, The University of Western Ontario, London, Ontario N6A 5B7, Canada

Received: July 2, 2009; Revised Manuscript Received: August 23, 2009

As a classical electron-deficient molecule with unique hydrogen bridge bonding, diborane has created considerable interest in the structural chemistry. We report here the first evidence of pressure-induced structural transformations of diborane probed by in situ Raman spectroscopy. At pressures around 4 GPa, diborane undergoes a liquid−solid phase transformation to a new high-pressure phase I with a possible structure similar to the low-temperature phase. When compressed to above 6 GPa, the spectral features, such as doubling of the lattice modes, appearance of several new internal modes, and emergence of a new ring stretch mode, indicate the structural transformation to another new high-pressure phase II. This phase has a possible extended network structure of higher hydrides of borane. At pressures above 14 GPa, diborane transforms to yet another high-pressure phase III. All of the observed pressure-induced structural transformations are completely reversible upon decompression.

I. Introduction

High-pressure investigations of dense hydrides have received considerable interest because these hydrogenous materials are predicted to undergo metallization and eventually become superconductors at significantly lower pressures than those required for solid hydrogen.[1] Recent high-pressure studies of silane (SiH_4) have shown that this compound has interesting metallic and even superconducting behavior at pressures above 60 GPa.[2−6] Another hydride of group IIIA elements, alane (AlH_3), has been investigated using the first-principles density functional theory, where a transformation to a semimetallic phase at 73 GPa was predicted.[7] High-pressure spectroscopic studies on another group IIIA hydride, decaborane ($B_{10}H_{14}$), have also reported transitions to a nonmolecular phase above 100 GPa.[8]

In addition to investigations on metallization, studies of hydrides under pressure are also of significance from the point of view of hydrogen storage applications. From simple binary to very complex hydrides, structural transformation at different temperatures and pressures has been a critical issue, the understanding of which will help to explore the feasibility of these hydrides with regard to their hydrogen storage capacities. Pressure- and temperature-induced structural transitions in various borohydrides such as $X(BH_4)_2$ (X = Ca, Mg, etc.)[9,10] and $Y(BH_4)$ (Y = Li, K, Rb, etc.)[11−13] have been reported in recent years. High-pressure investigations of ammonia borane (NH_3BH_3) have also revealed interesting structural transformations characterized by significant changes in the dihydrogen bonding interactions with pressure.[14,15]

Boron hydrides (i.e., boranes) are of interest, in particular, due to the rich chemistry associated with their unusual structures and versatile reactions accessible under different thermodynamical conditions.[16] Theoretical investigations on the electron correlation effects in the structures of boron hydrides have explored various possible intermediates and reactions involving various boranes.[17] Recently, computational studies on the stability of boron−hydrogen compounds using total energy calculations have predicted that binary B/H systems can become thermodynamically more stable at higher pressures relative to the covalent molecular boron hydrides observed at ambient conditions.[18] In addition, structures with an extended network of bonds or metallic bonding are found to be energetically favored at high pressures. For instance, single borane (BH_3) is anticipated to undergo a second-order structural transition at ∼5 GPa followed by a metal−insulator transition at ∼30 GPa. In addition, this hypothetical phase of borane that is stable at high pressures, if recovered at atmospheric pressure, is found not only to be energetic but to store 2.6 times more hydrogen per unit volume than cryogenic liquid H_2 itself. Therefore, it would be of interest to carry out high-pressure investigations on boranes to explore the high-pressure phases which are of relevance to fundamental chemistry as well as hydrogen storage applications.

While BH_3 is not stable under ambient conditions, diborane (B_2H_6)[19−21] is the simplest stable boron hydride among the other stable forms of boranes, such as tetraborane (B_4H_{10}),[22,23] pentaborane (B_5H_9),[24,25] decaborane ($B_{10}H_{14}$),[8] and so forth. Diborane is of conventional interest in the structural chemistry of boron as it is a classical electron-deficient molecule with peculiar hydrogen bridge bonding. Using electron diffraction on gaseous diborane, Bauer et al.[19] first reported that the B−B and B−H distances are larger than the corresponding values for the ethane model, thus pointing to the possibility of a bridge structure with one electron or no electron bonds. Later, the electron diffraction study of diborane was reinvestigated by Hedberg et al.,[20] and the bridge structure was further confirmed by Bartell et al.[21] The history of how the structure of diborane was understood can now be inferred from an essay by Laszlo.[26] The bridge structure of solid diborane was later solved by the Lipscomb group using X-ray diffraction studies.[27,28] At ambient pressure and below 60 K, solid diborane crystallizes into the α phase with an orthorhombic structure ($a = 7.89$, $b = 4.54$, and $c = 6.89$ Å and $Z = 4$), while annealing to above 90 K results in the formation of β phase (space group $P2_1/n$, $a = 4.40$, $b = 5.72$, and $c = 6.50$ Å and $\gamma = 105.1°$). The crystal structure of the β-phase diborane is shown in Figure 1. In addition, the

* To whom correspondence should be addressed. E-mail: yang.song@uwo.ca. Phone: (519)661-2111 ext. 86310. Fax: (519)661-3022.
[†] Permanent address: High Pressure Physics Division, Bhabha Atomic Research Centre, Mumbai, India 400085.

10.1021/jp906261s CCC: $40.75
Published on Web 09/18/2009

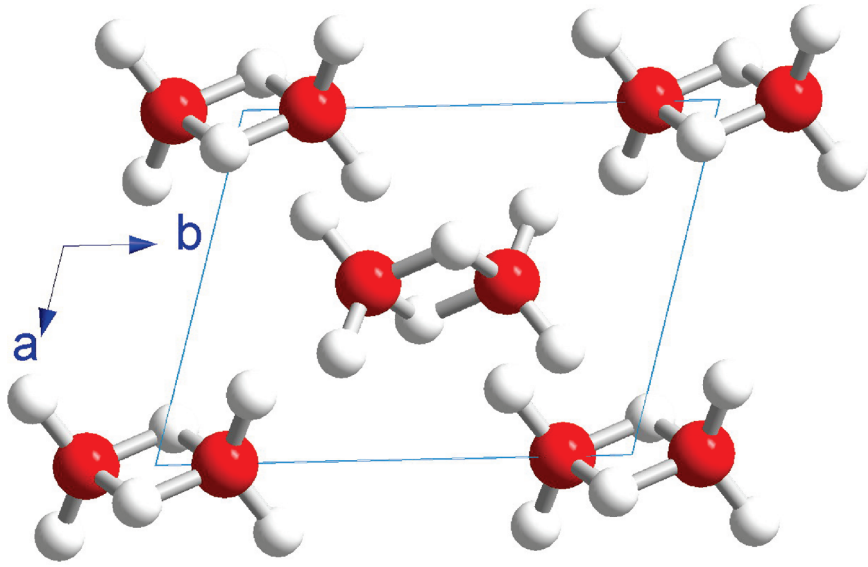

Figure 1. The crystal structure of β-diborane at ambient pressure and low temperature (e.g., 90 K). The rendering shows the *ab* crystal plane (e.g., normal to *c* axis). The bigger red balls denote the boron atom, and the small gray ones denote hydrogen atoms.

structures of diborane have been extensively characterized by vibrational spectroscopy both experimentally and theoretically.[27−32] Both Raman and infrared studies of diborane supported the well-established bridge structure.[29,30] The most recent vibrational assignments based on infrared (IR) measurements by Duncan et al.[31] are found to be consistent with several earlier IR and Raman spectroscopic observations of diborane.[32−39]

As diborane exists in the gaseous phase, experimental investigations even under ambient conditions are quite challenging. As a result, vibrational spectroscopic studies of this compound in the condensed phase at ambient temperature have not been reported so far. We report here the first Raman spectroscopic study of diborane at room temperature from a near-ambient pressure to pressures up to 24 GPa. In this study, we report the evidence of new high-pressure phases of diborane with implications of hydrogen storage applications.

II. Experimental Details

Gaseous diborane of electronic grade (purity 99.99%) packed in a lecture bottle with a 10% concentration balanced with hydrogen was purchased from Aldrich and used without further purification. Loading was done by precooling a diamond anvil cell (DAC) in liquid nitrogen. The melting point for B_2H_6 is −165 °C, and hence gaseous B_2H_6 solidifies on the rhenium gasket in the cell cooled in a liquid nitrogen bath. The cell was then sealed, and the solid B_2H_6 was pressurized before warming to room temperature. A few ruby chips were inserted for pressure measurements before the cryogenic loading. The pressure was determined from the well-established pressure shift of the R_1 ruby fluorescence line with an accuracy of ±0.05 GPa under quasi-hydrostatic conditions.[40] For the entire pressure region, ruby fluorescence spectra obtained on different ruby chips across the sample chamber indicate no significant pressure gradient, indicating B_2H_6 itself is an excellent pressure transmitting medium in the pressure region of current study.

Raman measurements were carried out with a customized Raman microspectroscopy system. The 488 nm line of an Innova Ar^+ laser from Coherent Inc. was used as the excitation source. The laser was focused to less than 5 μm on the sample with an average power of ∼30 mW by an Olympus microscope with a 20× objective. A 15× eyepiece and a digital camera allowed precise alignment of the focused laser beam on the sample. The Raman scattering signal was collected by the same objective lens with a backscattering geometry. The Rayleigh scattering was removed by a pair of notch filters, which enable a measurable spectral range above 100 cm^{-1}. The scattered photons were focused on the entrance slit of a spectrometer and then dispersed by an imaging spectrograph housing a 0.5 m focal distance monochromator equipped with multiple gratings. In this experiment, 1800 lines/mm grating with ±0.1 cm^{-1} resolution was used. The Raman signal was recorded by an ultrasensitive liquid-nitrogen-cooled, back-illuminated charge-coupled device (CCD) detector from Acton. The system was calibrated using neon lines with an uncertainty of ±1 cm^{-1}. All measurements were conducted at room temperature.

III. Results and Discussion

Although diborane has been characterized in the condensed phase by IR spectroscopy at low temperatures,[41] the corresponding Raman measurements are very limited. So far, Raman spectra of diborane have been recorded only for its liquid phase at −130 °C and only on a photographic plate using a mercury lamp.[29,33] Upon successful loading of diborane into a DAC, here we report the first laser-excited Raman spectra of condensed diborane at ambient temperature. Figure 2 depicts the Raman spectrum of diborane collected at room temperature and very low pressure (i.e., <1 GPa) in the liquid phase.

Single diborane has a D_{2h} molecular symmetry in both the gaseous and crystalline phases, and thus, the irreducible representation for molecular B_2H_6 is

$$\Gamma_{D_{2h}}(B_2H_6) = 4A_g + 2B_{1g} + 2B_{2g} + 1B_{3g} + 1A_u + 2B_{1u} + 3B_{2u} + 3B_{3u} \quad (1)$$

where all the gerade modes are Raman-active. In the crystalline phase (assuming the known β phase with space group $P2_1/n$), however, the factor group of the B_2H_6 crystal lattice has a lower symmetry C_{2h}, and thus, the irreducible representation for the lattice modes is

$$\Gamma^{\text{lattice}}_{C_{2h}}(B_2H_6) = 3A_g + 3B_g + 2A_u + B_u \qquad (2)$$

The $3A_g + 3B_g$ modes associated with lattice librations are Raman-active, while the remaining modes associated with lattice translations are IR-active. As seen from Figure 2, all nine predicted Raman-active internal modes are observed except for the ν_7 (B_{2g}) and ν_{12} (B_{1g}) modes associated with BH_2 wagging and rocking, respectively. The additional bands, especially those labeled with L, are likely combination bands exclusively associated with the liquid phase. Upon transformation to the solid phase, these bands faded away, as seen in Figure 3. Table 1 summarizes all of the observed modes at near-ambient conditions with assignment in comparison with those reported in the liquid phase by Lord et al.[33] and those in the crystalline phase derived from IR studies by Duncan et al.[31] Table 1 also listed the new modes that are observed at higher pressures and the pressure dependence (i.e., $d\nu/dP$ in cm^{-1}/GPa) of the Raman modes of the high-pressure phases.

Figure 3a shows selected Raman spectra of diborane in the spectral region of 100−1200 cm^{-1} at different pressures during compression, while the Raman shift versus pressure in this spectral region is shown in Figure 3b. Similarly, selected Raman spectra collected at the same pressures in the spectral regions of 1400−2400 and 2800−3200 cm^{-1} upon compression are depicted in Figures 4a and 5a, respectively, with the corresponding pressure dependence of the Raman modes shown in Figures 4b and 5b. Figure 6a, b, and c depicts selected Raman spectra of diborane upon decompression from the highest pressure.

A. Liquid Phase. The Raman spectra of diborane collected at less than 4 GPa in the spectral region of 100−1200 cm^{-1} shown in Figure 2 are very similar to the Raman spectra reported for liquid borane.[29,33] The broad-band profile of the observed Raman modes is characteristic of a liquid. The pressure-induced frequency shifts of these modes in the liquid phase are reported in Table 1. The ring deformation mode ν_4 (804 cm^{-1}) shows stiffening at a rate of 8.6 cm^{-1}/GPa and remains broad up to 4 GPa. The BH_2 twist mode ν_{15} (1025 cm^{-1}), however, exhibits prominent softening at a rate of −5.7 cm^{-1}/GPa. The terminal B−H symmetric deformation mode, ν_3 at 1182 cm^{-1}, shows a relatively lower rate of stiffening (2.6 cm^{-1}/GPa) with enhancing intensity as pressure increases. Similarly, the relative intensity of the antisymmetric ring stretch mode ν_6 (1791 cm^{-1}) increases with pressure. Both this mode and the ring symmetric stretch mode ν_2 (2105 cm^{-1}) show nearly the same stiffening rate of 7.9 cm^{-1}/GPa. Likewise, both the terminal B−H symmetric and antisymmetric stretching modes, ν_1 (2535 cm^{-1}) and ν_{11} (2599 cm^{-1}), stiffen at nearly the same rate of 12.9 cm^{-1}/GPa.

B. Liquid−Solid Transition: Phase I. The Raman spectra collected at 4 GPa as shown in Figures 3a, 4a, and 5a are characterized by the emergence of well-resolved lattice modes and sharpening of other internal Raman-active modes. These evolutions indicate that diborane has undergone a liquid−solid phase transition to a high-pressure phase, which we label as phase I. As can be seen from Table 1, the observed lattice modes in phase I at 179 and 222 cm^{-1} stiffen rapidly with pressure at a rate of 13.5 and 21.5 cm^{-1}/GPa, respectively. The stiffening rate for other Raman modes is also higher in this phase compared to other subsequent phases observed at higher pressures. These observations suggest that diborane is highly compressible in this pressure range. Some of the other notable spectral features around 4 GPa include that the ν_4 (ring deformation) mode significantly broadens and starts to split, while the BH_2 wagging mode ν_7 observed at 879 cm^{-1} becomes more prominent. Most of the observed modes show monotonic pressure-induced stiffening. Except for the emergence of the lattice modes and the ν_7 mode, there were no other new spectral features observed in this phase.

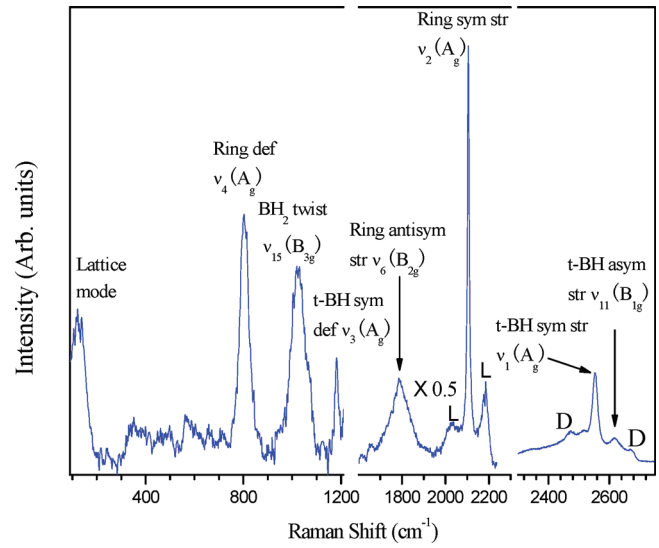

Figure 2. Raman spectrum of diborane collected at room temperature and low pressure in the liquid phase. The vibrational assignment is labeled above each mode. The spectral region of 1600−2300 cm^{-1} has been rescaled with 50% of the original intensity. L denotes the bands associated with the liquid phase, while D refers to the (second-order) Raman band of diamond.

C. Phase Transition above 6 GPa: Phase II. At pressures above 6 GPa, spectral changes are rather drastic, indicating substantial changes in the crystal and/or molecular structures. As shown in Figure 3a, two additional modes at 326 and 367 cm^{-1} are observed in the lattice region, resulting in the doubling of the number of the lattice modes. In addition, the ν_4 (ring deformation) mode and the ν_{15} (BH_2 twist) mode are found to split unambiguously. More prominently, several new internal modes appear in the spectral region of 800−1000 cm^{-1}, as listed in Table 1. As seen from Figure 4a, a new mode at 2063 cm^{-1} emerges adjacent to the symmetric ring stretch mode ν_2, and its intensity increases considerably upon further compression. The spectral features of this mode and especially the fact of its close proximity to the ν_2 mode suggest that it might be an additional ring stretch mode arising from a new ring or a cage structure. There were no dramatic changes in the spectral region for the *t*-BH symmetric and antisymmetric skeletal stretching modes, ν_1 and ν_{11} (Figure 5a). However, the stiffening rates for both of the modes showed a discontinuity across 6 GPa (Figure 5b). All of the above-mentioned spectral changes at this pressure indicate that diborane has undergone a phase transformation to a new high-pressure phase, which we label as phase II. This phase is found to be less compressible compared to the other phases as inferred from the relatively "flatter" pressure dependence of the Raman modes in this region, as shown in Figures 4b, 5b, and 6b with the corresponding lower $d\nu/dP$ values for this phase listed in Table 1. The absence of any softening of the *t*-BH stretching modes indicates that, unlike ammonia borane,[14] there is no enhancement of dihydrogen bonding interactions in diborane at higher pressures.

D. High-Pressure Phase III above 14 GPa. At pressures above 14 GPa, the lattice modes are found to become significantly broadened. In addition, the number of resolvable lattice modes above this pressure becomes two, similar to the initial high-pressure phase I. Moreover, the split ν_4 (ring deformation)

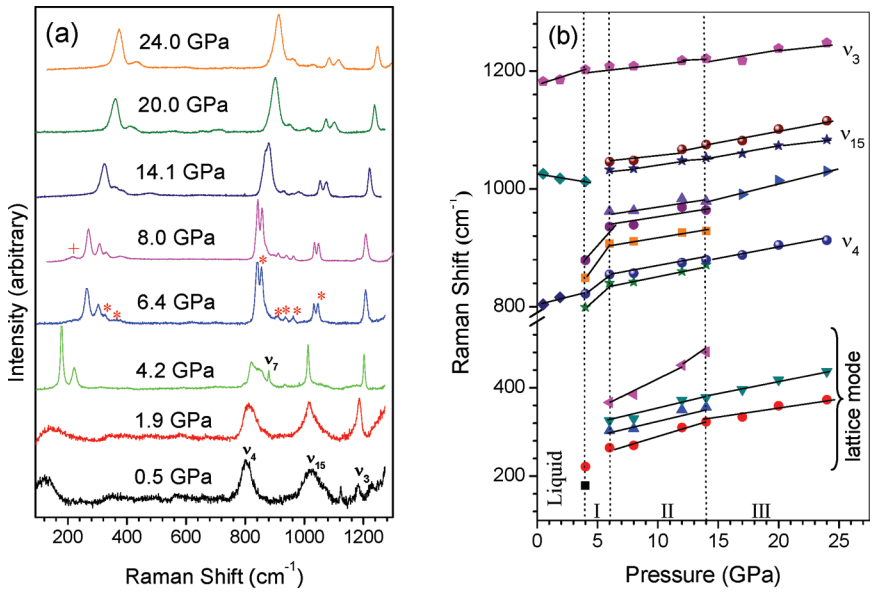

Figure 3. (a) Selected Raman spectra of diborane collected at room temperature upon compression in the spectral region of 100−1400 cm^{-1}. The asterisks represent the new modes observed upon compression. (b) Pressure dependence of Raman shifts of diborane for the modes in the region of 100−1300 cm^{-1}. Different symbols denote Raman modes with different origins. The solid lines crossing the solid symbols are for eye guidance. The vertical dashed lines indicate the proposed phase boundaries.

TABLE 1: Assignment of Observed Raman Modes of B_2H_6 at Different $P-T$ Conditions and Pressure Dependence of the Raman Shift for Each Mode

						dν/dP (cm^{-1}/GPa) [f]			
symmetry	mode[a]	description[a,b,c]	Duncan[a] (cm^{-1})	Lord[d] (cm^{-1})	this study[e] (cm^{-1})	liquid	I	II	III
A_g	ν_1	*t*-BH sym stretch	2523	2524	2535	12.9	15.5	2.0	9.0
	ν_2	ring sym stretch	2098	2104	2105	7.9	2.0	2.0	8.3
	ν_3	*t*-BH sym def	1173	1180	1182	2.6	2.7	1.3	6.7
	ν_4	ring def	798	794	804	8.6	16.5	0.5	7.3
B_{2g}	ν_6	ring antisym stretch	1743	1747	1791	7.9	5.5	0	4.7
B_{1g}	ν_{11}	*t*-BH antisym stretch	2586	2591	2599	12.9	18.0	0.5	11.7
B_{3g}	ν_{15}	BH_2 twist	1006	1011	1025	−5.7	10.0	1.0	4.3
new internal mode[g]					855		1.0	2.0	
					907		2.0	2.0	
					936			1.5	10.3
					962			0.5	7.7
					2063			1.5	11.7
lattice mode[h]					(179)		13.5	3.0	
					(222)		21.5	2.5	
					265			2.6	
					303			2.1	
					326			2.1	7.3
					367			8.5	8.3

[a] Reference 31. Obtained from IR measurements on crystalline diborane. [b] Reference 36. [c] Reference 38. [d] Reference 33. Obtained from Raman measurements on liquid diborane at −130 °C. [e] Observed at 0.5 GPa and room temperature in the liquid phase for all internal modes, unless otherwise indicated. [f] Obtained by linear fit of the Raman modes in four pressure regions, as indicated in the text and Figures 3b, 4b, and 5b. [g] Observed above 6.4 GPa. [h] The modes in the parentheses are observed at 4.2 GPa, and others are observed at 6.4 GPa.

mode below 14 GPa is found to merge into a single peak and thus also becomes broadened. In contrast, the ν_{15} (BH_2 twist) mode continues to remain a doublet up to the highest pressure of 24 GPa. The respective ring symmetric and asymmetric stretch modes, ν_2 and ν_6, show significant broadening at pressures above 14 GPa. The relative intensity of the new ring stretch mode (2063 cm^{-1}) adjacent to the symmetric ring stretch mode ν_2 is found to increase substantially across this pressure. All of the observed modes show discontinuous pressure dependence (i.e., dν/dP values) across 14 GPa. These observations suggest another structural transition to a high-pressure phase, which we label as III. No further spectral changes were observed upon compression to the highest pressure of the current study, that is, 24 GPa, indicating a broad stability region of this phase. Overall, this phase is characterized by a broadened and weakened band profile and the reduction of the number of Raman-active modes.

E. Raman Spectra upon Decompression. The Raman spectra of diborane in the entire spectral region have been recorded upon decompression as well. Figure 6a, b, and c shows the Raman spectra in the spectral regions of 200−1200, 1400−1800, and 2400−2800 cm^{-1} with decreasing pressure. When decompressed from ~24 GPa, diborane transforms back to high-pressure phase II at pressures less than 14 GPa. This transition is most evidenced by the drastic reduction in the intensity of the new mode observed adjacent to the ring stretch

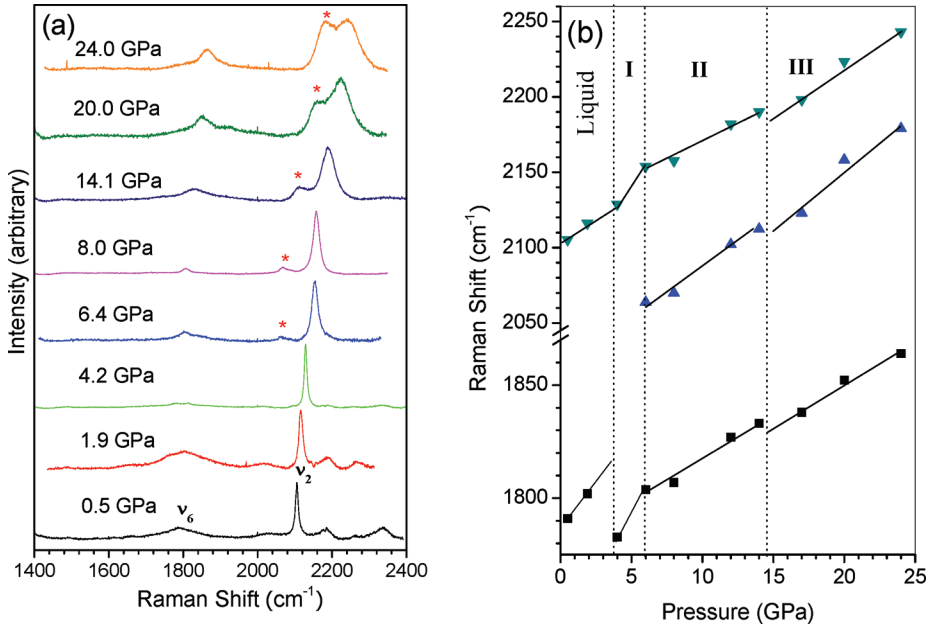

Figure 4. (a) Selected Raman spectra of diborane collected at room temperature upon compression in the spectral region of 1400−2400 cm^{-1}. The asterisks represent the new modes observed upon compression. (b) Pressure dependence of Raman shifts of diborane for the ν_6, ν_2, and the new modes in this spectral region. Other legends follow those of Figure 3b.

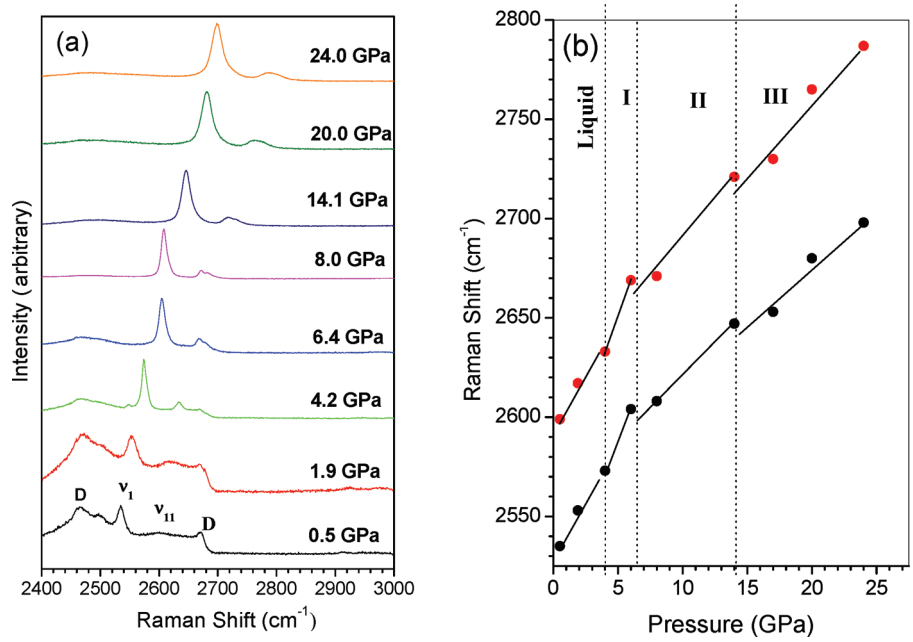

Figure 5. (a) Selected Raman spectra of diborane collected at room temperature upon compression in the spectral region of 2400−3000 cm^{-1}. D represents the (second-order) Raman band from diamond. (b) Pressure dependence of Raman shifts of diborane for the ν_1 and ν_{11} modes in this spectral region. Other legends follow those of Figure 3b.

mode. Further decompression results in the reduction of the intensity of this mode until 0.5 GPa, when this mode is completely depleted. The next back transformation, that is, solid phase III to II is observed at around 5.3 GPa as characterized by the doubling of the number of the lattice modes and the splitting of the ring deformation mode ν_4. At pressures lower than 3 GPa, the lattice modes disappear while the sharp internal modes are replaced by broad bands which are characteristic of the liquid phase of diborane observed before compression. The Raman spectra of diborane retrieved under near-ambient conditions are very similar to those of the starting liquid phase. Therefore, all of the observed pressure-induced structural changes are completely reversible.

F. Discussion. As described above, we observed rich pressure-induced transformations of diborane and identified three new solid phases in addition to the previously observed two low-temperature phases, that is, the α and β phases. For substances with "normal" melting curve (i.e., the melting point increases with pressure), cooling down and compression in a small $P-T$ region often produce equivalent solid phases. The solid phase I of diborane observed at 4−6 GPa, therefore, has a possibly similar structure as the β phase, that is, with the same point group symmetry, although the detailed space group might be different. Indeed, a recent X-ray diffraction study on ammonia borane shows that the room-temperature and high-pressure phase (space group $Cmc2_1$) is very similar to the low-temperature

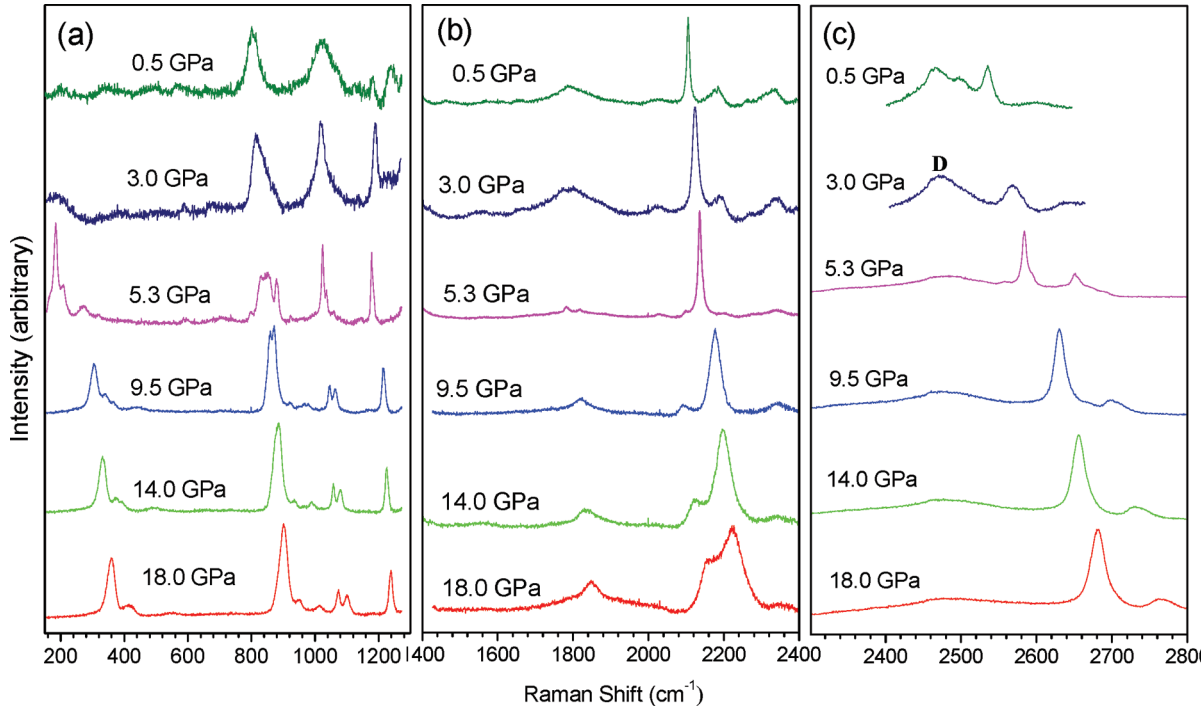

Figure 6. Selected Raman spectra of diborane collected at room temperature upon decompression in the spectral region of (a) 100−1300 cm^{-1}, (b) 1400−2400 cm^{-1}, and (c) 2300−2800 cm^{-1}. D in (c) represents the (second-order) Raman band of diamond.

ambient-pressure phase (space group $Pmn2_1$), that is, with the same C_{2v} point group symmetry.[42] The two lattice modes are consistent with a C_{2h} crystal lattice and could be a subset of the six predicted librational modes (i.e., $3A_g + 3B_g$). The dramatically different lattice patterns observed between 6 and 14 GPa, however, strongly suggest that the crystal structure of the solid phase II is significantly different from that of phase I. The extremely large pressure-induced shift of the two dominant lattice modes from 4.2 to 6.4 GPa (Figure 6), that is, from 179 and 222 cm^{-1} to 264 and 303 cm^{-1}, suggests that they are highly unlikely to originate from the same crystal structure. The additional lattice modes observed could be infrared-active modes, thus pointing to a noncentrosymmetric factor group of the new crystal lattice, which possibly has a lower symmetry, such as C_{2v}. Above 14 GPa, the number of lattice modes for solid phase III is reverted to two, and the lattice region is similar to that for phase I. Therefore, the factor group for phase III is likely similar to phase I, although the detailed crystal structure and space group symmetry might be different. The broadening of all Raman modes, especially in the lattice region, suggests that phase III may eventually transform to a disordered phase upon further compression. All of these spectroscopic analyses of the structures of high-pressure phases of diborane need to be verified by X-ray or neutron diffraction measurements.

Furthermore, the structural chemistry of borane is of fundamental interest particularly at high pressures due to the possible observation of novel structures and reactions predicted by theories.[18] Under ambient conditions, theoretical investigations have explored various possible intermediates and reactions involving diborane, such as the dissociation of B_2H_6 to $2BH_3$ or reaction of $2B_2H_6$ to form $BH_3 + B_3H_9$ or the formation of tetramers of borane $(BH_3)_4$ or the dimer of diborane $(B_2H_6)_2$.[17,43] As electron density can be tuned more effectively with rapidly reducing volumes upon compression, pressure-induced chemical reactions are highly possible. For instance, at pressures above 6 GPa, drastic spectral changes, especially the observation of abundant new internal modes, strongly suggest enhanced intermolecular interaction with covalent nature. At higher pressures, however, the mobility of the atoms is restricted, and hence, the most facilitated phase transformations are the ones which are not associated with large atomic movements. The formation of higher hydrides is therefore possible without drastic changes in the atomic positions. Moreover, our spectroscopic observations, such as the emergence of new modes in the spectral region of ring deformation and a new band adjacent to the ring stretch mode, could be attributed to a new high-pressure structure characterized by a network of higher hydrides, that is, one of the tetramer forms of borane.[44] Among these possible structures of tetramers (e.g., B_4H_{12}), the deformed ring structure with bend B−H−B bridges with a C_{2v} symmetry has been reported to have a local minimum. This structure is closely related to the butterfly structure, a possible stable structure of the known tetraborane-10 (B_4H_{10}) .[44]

Although the stable B_4H_{10} may be formed in the high-pressure phase II among other possible tetramer forms of borane, its formation is less likely for two reasons. First, our spectroscopic studies find no evidence of the evolution of free hydrogen, which is expected as a byproduct of the chemical reaction below

$$B_2H_6 + B_2H_6 \rightarrow B_4H_{10} + H_2 \qquad (3)$$

Moreover, the fact that this high-pressure phase transforms back to the initial solid high-pressure phase I upon decompression suggests that this new phase II observed at higher pressures is not stable under ambient conditions. Since tetraborane-10 is known to have certain stability at ambient conditions, pressure-induced conversion to B_4H_{10} would have been probably irreversible. Thermodynamically, hydrogen release via reaction (3) is only slightly nonspontaneous at ambient conditions (i.e., $\Delta G = +9.2$ kJ mol^{-1}),[16] while at high pressures, the forward reaction might be favored. However, under diamond anvil cell conditions where the production of hydrogen may result in significant change of volume, the thermodynamics of the above

reaction at high pressures might be substantially different, such that hydrogen release is suppressed. In addition, it is highly likely that the formation of B_4H_{10} may be kinetically hindered and thus may require a higher temperature than ambient. The other possible tetramer, tetraborane-12 (B_4H_{12}), however, is far from stable at ambient conditions ($\Delta G_f = +335$ kJ mol^{-1}).[16] Except for the theoretical computations, unfortunately, no experimental data on the structural or spectral details are available for this tetramer, especially at high pressures. However, the doubling of the lattice modes observed at 6.4 GPa might also be a result of the doubling of the unit cell content associated with a molecular arrangement that resembles higher hydrides of boranes. Apparently, theoretical computations of the possible high-pressure phases of diborane, and eventually the structural investigations using X-ray or preferably neutron diffraction measurements, would be very useful to elucidate our Raman observations and especially the crystal and molecular structure of phase II formed at around 6 GPa.

If the observed high-pressure phase II above 6 GPa is found to be a network structure of higher hydrides, this would constitute a new member of the borane family. Similar to pentaborane, this network or caged borane structure may be of great relevance to hydrogen storage applications. Our high-pressure studies indicate that this high-pressure phase II is not stable under ambient conditions, and the high-pressure phase is found to be completely reversible. However, temperature variations, especially low temperatures, may greatly enhance the stability or metastability of the phase II. Furthermore, if loaded along with free hydrogen and compressed to higher pressures, a network or a cage structure might be stabilized by the borane−hydrogen complex and be recoverable under certain conditions, making diborane a potential precursor to produce hydrogen storage materials.

IV. Conclusions

Raman spectroscopic investigations of diborane at room temperature have been carried out up to 24 GPa. Diborane is found to exist in the liquid phase up to pressures of less than 4 GPa. Above this pressure, it undergoes a liquid−solid phase transition to a high-pressure phase I which resembles the low-temperature phase of diborane. At pressures above 6 GPa, it transforms to a distinct new high-pressure phase II characterized by a possible network of higher hydrides, which presents the potential for possible hydrogen storage applications. Above 14 GPa, diborane undergoes another structural phase transition to high-pressure phase III, which is stable up to 24 GPa, the highest pressure of the current study. Upon release of pressure from 24 GPa, pressure-induced transformations are found to be completely reversible. The detailed structures of these new phases identified in our spectroscopic measurements require further computational support as well as diffraction measurements.

Acknowledgment. Y.S. acknowledges support from a Discovery Grant and a RTI Grant from the NSERC of Canada, a Leaders Opportunity Fund from the Canadian Foundation for Innovation, and an Early Researcher Award from the Ontario Ministry of Research and Innovation. C.M. acknowledges the CCP fellowship from UWO.

References and Notes

(1) Ashcroft, N. W. *Phys. Rev. Lett.* **2004**, *92*, 187002.
(2) Feng, J.; Grochala, W.; Jaroń, T.; Hoffmann, R.; Bergara, A.; Ashcroft, N. W. *Phys. Rev. Lett.* **2006**, *96*, 017006.
(3) Martinez-Canales, M.; Oganov, A. R.; Ma, Y.; Yan, Y.; Lyakhov, A. O.; Bergara, A. *Phys. Rev. Lett.* **2009**, *102*, 087005.
(4) Chen, X.-J.; Struzhkin, V. V.; Song, Y.; Goncharov, A. F.; Ahart, M.; Liu, Z.; Mao, H.-K.; Hemley, R. J. *Proc. Natl. Acad. Sci. U.S.A.* **2008**, *105*, 20–23.
(5) Eremets, M. I.; Trojan, I. A.; Medvedev, S. A.; Tse, J. S.; Yao, Y. *Science* **2008**, *319*, 1506–1509.
(6) Kima, D. Y.; Scheicher, R. H.; Lebegue, S.; Prasongkit, J.; Arnaud, B.; Alouani, M.; Ahuja, R. *Proc. Natl. Acad. Sci. U.S.A.* **2008**, *105*, 16454–16459.
(7) Pickard, C. J.; Needs, R. J. *Phys. Rev. B* **2007**, *76*, 144114.
(8) Nakano, S.; Hemley, R. J.; Gregoryanz, E. A.; Goncharov, A. F.; Mao, H. *J. Phys.: Condens. Matter* **2002**, *14*, 10453–10456.
(9) Filinchuk, Y.; Roñnebro, E.; Chandra, D. *Acta Mater.* **2009**, *57*, 732–738.
(10) Geoge, L.; Vadym, D.; Saxena, S. K. *J. Phys. Chem. C* **2009**, *113*, 486.
(11) Talyzin, A. V.; Andersson, O.; Sundqvist, B.; Kurnosov, A.; Dubrovinsky, L. *J. Solid State Chem.* **2007**, *180*, 510–517.
(12) Kumar, R. S.; Kim, E.; Cornelius, A. L. *J.Phys. Chem. C* **2008**, *112*, 8452–8457.
(13) Kumar, R. S.; Cornelius, A. L. *J. Alloys Compd.* **2009**, *476*, 5–8.
(14) Xie, S.; Song, Y.; Liu, Z. *Can. J. Chem.* **2009**, *87*, 1235.
(15) Lin, Y.; Mao, W. L.; Drozd, V.; Chen, J.; Daemen, L. L. *J. Chem. Phys.* **2008**, *128*, 234509.
(16) Yu, C.-L.; Bauer, S. H. *J. Phys. Chem. Ref. Data* **1998**, *27*, 807–835.
(17) Lipscomb, W. N. *Pure Appl. Chem.* **1983**, *55*, 1431.
(18) Barbee, T. W., III; McMahan, A. K.; Klepeis, J. E.; Van Schilfgaarde, M. *Phys. Rev. B* **1997**, *56*, 5148–5155.
(19) Bauer, S. H. *J. Am. Chem. Soc.* **1937**, *59*, 1096–1103.
(20) Hedberg, K.; Schomaker, V. *J. Am. Chem. Soc.* **1951**, *73*, 1482–1487.
(21) Bartell, L. S.; Caeroll, B. L. *J. Chem. Phys.* **1965**, *42*, 1135–1139.
(22) Dahl, A. J.; Taylor, R. C. *Inorg. Chem.* **1971**, *10*, 2508–2515.
(23) Brain, P. T.; Morrison, C. A.; Parsons, S.; Rankin, D. W. H. *J. Chem. Soc.* **1996**, *24*, 4589–4596.
(24) Nordman, C. E. *J. Mol. Struct.* **1999**, *485−486*, 299–303.
(25) Beall, H.; Gaines, D. F. *Collect. Czech. Chem. Commun.* **1999**, *64*, 747–766.
(26) Laszlo, P. *Angew. Chem., Int. Ed* **2000**, *39*, 2071.
(27) Smith, H. W.; Lipscomb, W. N. *J. Chem. Phys.* **1965**, *43*, 1060–1064.
(28) Jones, D. S.; Lipscomb, W. N. *J. Chem. Phys.* **1969**, *51*, 3133–3134.
(29) Anderson, T. F.; Burg, A. B. *J. Chem. Phys.* **1938**, *6*, 586–591.
(30) Stitt, F. *J. Chem. Phys.* **1941**, *9*, 780–785.
(31) Duncan, J. L.; McKean, D. C.; Torto, I.; Nivellini, G. D. *J. Mol. Spectrosc.* **1981**, *85*, 16–39.
(32) Webb, A. N.; Neu, J. T.; Pitzer, K. S. *J. Chem. Phys.* **1949**, *17*, 1007–1011.
(33) Lord, R. C.; Nielsen, E. *J. Chem. Phys.* **1951**, *19*, 1–10.
(34) Taylor, R. C.; Emery, A. R. *Spectrochim. Acta* **1958**, *10*, 419–422.
(35) Carreira, L. A.; Odom, J. D.; Durig, J. R. *J. Chem. Phys.* **1973**, *59*, 4961–4965.
(36) Duncan, J. L.; Harper, J.; Hamilton, E.; Nivellini, G. D. *J. Mol. Spectrosc.* **1983**, *102*, 416–440.
(37) Duncan, J. L. *J. Mol. Spectrosc.* **1985**, *113*, 63–76.
(38) Vijay, A.; Sathyanarayana, D. N. *J. Mol. Struct.* **1995**, *351*, 215–229.
(39) Doménech, J. L.; Bermejo, D.; Flaud, J.; Lafferty, W. J. *J. Mol. Spectrosc.* **1999**, *194*, 185–188.
(40) Mao, H. K.; Xu, J.; Bell, P. M. *J. Geophys. Res.* **1986**, *91*, 4673.
(41) Freund, I.; Halford, R. S. *J. Chem. Phys.* **1965**, *43*, 3795.
(42) Filinchuk, Y.; Nevidomskyy, A. H.; Chernyshov, D.; Dmitriev, V. *Phys. Rev. B* **2009**, *79*, 214111.
(43) Stanton, J. F.; Bartlett, R. J.; Lipscomb, W. N. *Chem. Phys. Lett.* **1987**, *138*, 525–530.
(44) Shen, M.; Liang, C.; Schaefer III, H. F. *Chem. Phys.* **1993**, *171*, 325–345.

JP906261S